Overcoming the uplink limit of satellite-based quantum communication with deterministic quantum teleportation

Zhiyue Zuo,[1] Yijun Wang,[1] Qin Liao,[2,*] and Ying Guo[1]
[1]*School of Automation, Central South University, Changsha 410083, China*
[2]*College of Computer Science and Electronic Engineering, Hunan University, Changsha 410082, China*

(Received 21 April 2021; accepted 19 August 2021; published 31 August 2021)

Satellite-based quantum communication is essential for both foundational quantum physics tests and scalable quantum networks. However, the practical implementation of such application is limited due to the turbulent atmosphere, which is especially challenging for the ground-to-satellite uplink scenario. Here we consider the configuration of the continuous-variable quantum teleportation protocol to overcome both the uplink limit and background-radiation constraints with an unconditional and deterministic transfer, where the propagation of quantum light is affected by the favorable satellite-to-ground downlink (including the effects of absorption, scattering, turbulence, pointing errors, and background light). In particular, we derive the turbulent-induced fidelity that is achievable by the protocol for both nighttime and daytime operations, showing the effectiveness of this approach for various squeezing levels and orbit conditions (satellite altitudes and zenith angles). Finally, several approaches for fidelity enhancement are suggested, in terms of optimizing the transmitted Gaussian entanglement in the free-space scenario.

DOI: 10.1103/PhysRevA.104.022615

I. INTRODUCTION

One of the most famous applications of quantum mechanics is the capability to achieve theoretically unconditional secure communication even against adversaries with a quantum computer [1]. In recent decades, a number of quantum protocols have been successfully realized, including quantum teleportation (QT) [2], quantum key distribution (QKD) [3–5], quantum secret sharing [6], quantum clock synchronization [7], and distributed quantum metrology and sensing [8]. Further efforts in this research community have considered realizing a real-world quantum network on a global scale.

Unfortunately, the transmission distance of a ground-based quantum protocol (based on optical fibers) was limited to moderate distances due to huge channel losses, and the quantum signal fails to be measured precisely or replicated perfectly [9]. To achieve a global-scale quantum network, the transmission distance needs to be greatly lengthened. One solution to this problem is the protocol of quantum repeaters (QRs) [10], which divides the transmission path into several segments along which errors and loss are corrected by using entanglement swapping [11] and entanglement purification [12]. However, the realization of expensive QRs remains experimentally challenging, such as the capabilities of long storage time and high retrieval efficiency [13]. In QKD Lucamarini *et al.* introduced an alternative scheme of QRs to overcome the rate-distance limit [14], but it also needs a chain of trusted nodes for a global scale. The more nodes there are in such a network, the more serious challenges that security could be compromised are [15].

In view of the above, another promising solution is the use of orbiting satellites to transfer information among ground stations. The satellite, acting as a trusted and fast-moving node, can physically connect two separated points on Earth with reduced link loss since the extinction and turbulence mainly occur in the first 20 km of the atmosphere layer [16]. Several schemes for satellite-based quantum communication with current technology have been developed for satellite-to-ground downlink, ground-to-satellite uplink, or both [17–20]. To date, researchers have mainly focused on the downlink scenario because of its favorable transmission. Under comparable atmospheric conditions, the uplink geometry suffers more severe beam wandering and diffraction-induced broadening than downlink because the turbulence acts on the early stages of optical signal transmission [21]. In [22], Bourgoin *et al.* pointed out that the secret key rate in uplink QKD is less than one order of magnitude compared with the downlink scenario. Even with its challenges, however, the uplink geometry is also of great value since the information needs to transfer to the satellite node through an uplink, acting as an essential building block for a complete global-scale quantum network.

To overcome the uplink limit, Pugh *et al.* upgraded the uplink protocol with well-known adaptive optics (AO) techniques to reduce the detrimental effects of turbulence [23]. But the AO-based system in the real world is limited by the tight space and power of a satellite, for which much effort is devoted to satellite design, data storage or processing, and the accessibility for maintenance and repair [24]. Furthermore, Oliker and Gruneisen showed that the point-ahead angle of the uplink system will lead to imperfect wave-front compensation of AO and, as consequence, larger coupling attenuation at the receiver [25]. Although the authors reduced such attenuation by increasing the telescope diameter to 1 m, it is not realistic

*llqqlq@hnu.edu.cn

to have a 1-m telescope on a quantum satellite at this time; for example, Micius has a 30-cm telescope on board [17], and QEYSSAT is designed to have a 40-cm one [26].

In this scenario, the QT protocol, which allows an unknown quantum state to perform disembodied transportation from one object to another, opens a way for new opportunities. Recently, it was reported that the QT protocol overcomes the uplink limit of quantum communication via the downlink channel in the Micius platform [19]. There, the authors put the entanglement source at Micius and finished the transmission from ground to satellite through the favorable downlink. However, that analysis was based on a discrete-variable (DV) scheme, which prepared photonic qubits with probabilistic generation; therefore, it is hard to provide instantaneous transfer of quantum states without postselection [27]. Moreover, both background light and gravity affect the detection of photons, adding additional noise to the satellite-based DV system [28,29]. Alternatively, a continuous-variable (CV) scheme [30,31], using entangled states described in phase space, can realize unconditional and deterministic transfer since the generation, manipulation, and detection of continuous variables are unconditionally complete [32]. In addition, coherent detection with a bright local oscillator (LO) acting as a filter can reduce the background noise [33], while the influence of gravity on the signal could be compensated by employing a LO reference, which is affected in the same way [28].

Motivated by the findings above, in this paper, we establish the theoretic analysis of a continuous-variable quantum teleportation (CVQT) protocol based on the Braunstein-Kimble (BK) scheme [34] from a ground observatory to a low-Earth-orbit satellite. This scenario involves more general models for the physical processes occurring within the atmosphere (extinction, scattering, and turbulence) and descriptions for the background noise from sunlight. Accounting for these models, average fidelity, the figure of merit in a free-space protocol, is analyzed under various satellite altitudes together with nighttime and daytime operations. We show that the uplink QT with continuous variables is feasible for both night and day. Finally, we show here the average fidelity can be further improved by enhancing the Gaussian entanglement of entangled states.

This paper is organized as follows. In Sec. II, we suggest the structure of CVQT and show its fidelity model in a fading channel. In Sec. III, the atmosphere transmittance and excess noise of satellite-mediated links are demonstrated, and the fidelity for such a link is subsequently derived. In Sec. IV, enhanced strategies are suggested to improve the performance of CVQT. Finally, we draw a conclusion in Sec. V.

II. BK-BASED CVQT IN A FADING CHANNEL

In what follows, we introduce the notion of the CVQT protocol over a fading channel. Here we first use the BK standard scheme for easy understanding and then extend it in Sec. IV. We believe this route will be more favorable for readers since we mainly focus on overcoming the uplink limit, rather than a new teleportation scheme.

The schematic for CVQT via a satellite-to-ground downlink is shown in Fig. 1 (without the blue blocks). To teleport an unknown quantum state from ground to satellite without an uplink limit, Bob (satellite) holds the Einstein-Podolsky-Rosen (EPR) source. For a simple and convenient evaluation of fidelity, we describe the framework by its characteristic function (CF) representation [35]. This scheme can be described as follows.

(1) *EPR preparation.* Bob prepares an ideal EPR state generated from a pair of degenerate optical parametric amplifiers operating below their oscillation threshold [27], which can be described by its CF

$$\Phi_{\mathrm{EPR}}(\xi_a,\xi_b)=\exp(\Gamma\mathcal{U}\Gamma^{\dagger}), \tag{1}$$

where $\Gamma=(\xi_a^*,\xi_a,\xi_b^*,\xi_b)$ and $\mathcal{U}$ is the covariance matrix given by

$$\mathcal{U}=\begin{bmatrix}\cosh(2r)\mathbf{I} & \sinh(2r)\mathbf{R}\\ \sinh(2r)\mathbf{R} & \cosh(2r)\mathbf{I}\end{bmatrix}, \tag{2}$$

where r denotes the squeezing parameter, $\mathbf{I}=\mathrm{diag}(1,1)$, and $\mathbf{R}$ has the form

$$\mathbf{R}=\begin{bmatrix}0 & -1\\ -1 & 0\end{bmatrix}. \tag{3}$$

(2) *EPR correlation.* Alice (ground station) establishes the correlation with Bob via a transmitted EPR state. In particular, Bob leaves mode b of the EPR state locally, while the transmitted mode (mode a) passes through the favorable downlink. The major characteristics of the downlink are described by transmittance η and excess noise ϵ. Then, the CF of the transmitted EPR state is given by

$$\Phi(\xi_a,\xi_b)=\exp\left(-\frac{\Gamma\mathcal{U}_1\Gamma^{\dagger}}{4}\right), \tag{4}$$

with the covariance matrix

$$\mathcal{U}_1=\begin{bmatrix}A\mathbf{I} & C\mathbf{R}\\ C\mathbf{R} & B\mathbf{I}\end{bmatrix}, \tag{5}$$

where $A=\eta\cosh(2r)-\eta+1+\epsilon$, $B=\cosh(2r)$, and $C=\sqrt{\eta}\sinh(2r)$. Here the channel of mode b is assumed to be an ideal one without losses and excess noise.

(3) *Bell measurement.* Alice combines the input state with mode a via a balanced beam splitter (BS) and performs a CV Bell measurement with a pair of homodyne detections with LO. The input state is destroyed by the joint measurement with the measured quadratures $x_+=(x_{\mathrm{in}}+x_a)/\sqrt{2}$ and $p_-=(p_{\mathrm{in}}-p_a)/\sqrt{2}$. Here we consider an ideal homodyne detection for Bell measurement, and the analysis with imperfect detection is shown in [36].

(4) *Displacement.* The measured quadratures x_+ and p_-, which are used for coherent displacement on mode b, i.e., $x_b\to x_b+\sqrt{2}x_+$ and $p_b\to p_b+\sqrt{2}p_-$, are broadcast to Bob via the classical channel. In particular, Bob implements a translation for mode b by coupling a coherent beam with a 98:2 BS, which is modulated by x_+ and p_-, respectively, via an amplitude modulator and a phase modulator [27]. Finally, Bob retrieves the input state at the ground station, which can be expressed as

$$\Phi_{\mathrm{out}}(\xi)=\Phi_{\mathrm{in}}(\xi)\Phi(\xi^*,\xi), \tag{6}$$

where $\Phi_{\mathrm{in}}(\xi)$ and $\Phi_{\mathrm{out}}(\xi)$ denote the CF of the input state and output state, respectively.

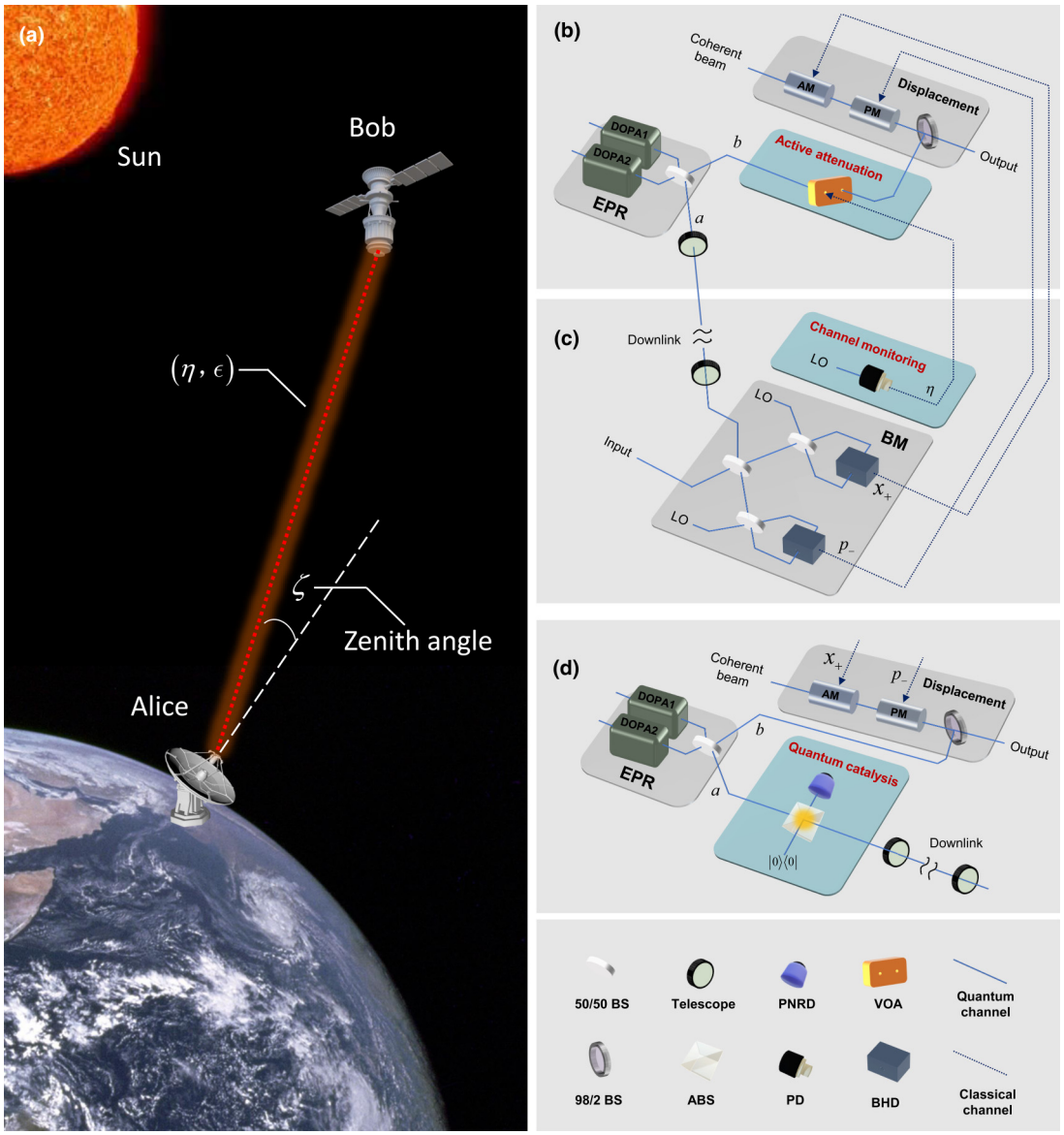

FIG. 1. Ground-to-satellite CVQT via downlink. (a) Overview of the ground-to-satellite CVQT. The downlink is characterized by atmospheric transmittance η and excess noise ϵ. (b) The setup of the active-attenuation scheme on the satellite. EPR, Einstein-Podolsky-Rosen state; DOPA, degenerate optical parametric amplifier; AM, amplitude modulator; PM, phase modulator. (c) The setup of the active-attenuation scheme at the ground station. The Bell measurement results (x_+ and p_-) and the real-time transmittance measured by the channel monitoring module are sent to the satellite through the classical communication channel. LO, local oscillator; BM, Bell measurement. (d) The setup of the quantum catalysis scheme on the satellite. BS, beam splitter; PNRD, photon-number-resolving detection; VOA, variable optical attenuator; ABS, asymmetrical beam splitter; PD, photodetector; BHD, balance homodyne detector.

As shown in the descriptions above, CVQT can realize an unconditional and deterministic transfer since the generation, manipulation, and detection of continuous variables are unconditionally complete. In contrast, the DV protocol experiences an obstacle in deterministic teleportation due to its probabilistic generation method [19]. In addition, CVQT waives the expensive single-photon detection (SPD) of the DV protocol, thereby avoiding the cooling problem of SPD at the same time [37]. Thus, the CV protocol is more suitable than a DV-based one for the requirements of building a network with nanosatellite [38].

Next, we demonstrate the fidelity of CVQT. Here we consider the case where the input state is a coherent state. The fidelity $\mathcal{F}$ denotes the closeness of the original and teleported states [39] and takes a value between 0 and 1, corresponding to orthogonal and identical states, respectively. Mathematically, the fidelity under the CF representation is given by

$$\mathcal{F} = \frac{1}{\pi}\int d^2\xi\, \Phi_{\text{in}}(\xi)\Phi_{\text{out}}(-\xi). \tag{7}$$

For coherent-state teleportation, $\mathcal{F}$ can be derived by the blocks of the covariance matrix in Eq. (5), given by [40]

$$\mathcal{F} = \frac{2}{\sqrt{\det D}}, \tag{8}$$

TABLE I. The simulation parameters in this work.

Variable	Value	Description	Reference
ζ	0°–60°	Zenith angle	
H	100, 300, 500 km	Satellite altitude	
C_n^2 (nighttime)	1.12×10^{-16} m$^{-2/3}$	Refraction-index structure parameter	
C_n^2 (daytime)	1.64×10^{-16} m$^{-2/3}$	Refraction-index structure parameter	
n_0 (nighttime)	0.61 m^{-3}	Mean number of scatterer particles	
n_0 (daytime)	0.01 m^{-3}	Mean number of scatterer particles	
β	0.7	Extinction coefficient	[16]
λ	800 nm	Wavelength	[44]
w_0	80 mm	Initial beam radius	[45]
a	1 m	Receiver telescope radius	[46]
α	0.4 μrad	Boresight error	[47]
H_b (nighttime)	1.5×10^{-5} W m^{-2} Sr μm	Typical brightness	[48]
H_b (daytime)	1.5 W m^{-2} Sr μm	Typical brightness	[48]
B_{filter}	0.01 nm	Filter bandwidth	[48]
Ω_{fov}	π	Field of view	[46]

where $D = (2 + A + B - 2C)\mathbf{I}$. Therefore, we have the fidelity given by

$$\mathcal{F} = \frac{2}{3 - \eta + (\eta + 1)\cosh(2r) - 2\sqrt{\eta}\sinh(2r) + \epsilon}. \quad (9)$$

Note that we select a vacuum state as the input state in the calculation. This is possible because the teleportation fidelity is the same for all coherent states, or in other words, the teleportation is invariant under displacement transformation [41].

Equation (9) denotes the fidelity under deterministic losses. However, the turbulent-induced downlink is a fading channel with fluctuating losses. Hence, the above-derived fidelity should take the loss fluctuation into account. Fortunately, the loss fluctuation, or, equivalently, the transmittance fluctuation, can be characterized by the probability density function of transmittance $\mathcal{P}(\eta)$ [42]. This is because the transmittance can be considered real random variables because of the negligible depolarization of the atmosphere [43]. With the support of $\mathcal{P}(\eta)$, the resulting input-output relations of a fading channel can be given by (see the Supplemental Material in Ref. [42])

$$\tilde{\Phi}_{\text{out}}(\xi) = \int_0^1 d\eta \mathcal{P}(\eta)\tilde{\Phi}_{\text{in}}(\eta\xi), \quad (10)$$

where $\tilde{\Phi}_{\text{in}}(\xi)$ and $\tilde{\Phi}_{\text{out}}(\xi)$ denote the CF of the field before and after the fading channel, respectively. Correspondingly, the fidelity under fluctuating transmittance can be derived by averaging the determined fidelity in Eq. (9) with $\mathcal{P}(\eta)$, which is given by

$$\mathcal{F}_{\text{ave}} = \int_0^1 d\eta \mathcal{F}\mathcal{P}(\eta). \quad (11)$$

Note that Eq. (11) is also treated for other fading channels, such as a horizontal free-space link or an ocean turbulent channel.

III. SIMULATION RESULTS

In this section, we derive the downlink characteristics for atmosphere transmittance and excess noise and then demonstrate the fidelity during both nighttime and daytime operation. Note that, for a simple and convenient discussion, we consider a scenario with clear weather and without fog or rain. The simulation parameters in the following are shown in Table I.

A. Transmittance

In the following, we work with $\mathcal{P}(\eta)$ via the elliptic-beam model [49] with regular extinction. The elliptic-beam model (see Fig. 2) takes into account the beam wandering, beam broadening, and deformation (assume an elliptic deformation) of a Gaussian beam caused by the atmosphere and has good agreement with experimental results. In the elliptic-beam model, $\mathcal{P}(\eta)$ has the form

$$\mathcal{P}(\eta) = \frac{2}{\pi}\int_{\mathbb{R}^4} d^4\Theta \int_0^{\frac{\pi}{2}} d\varphi \rho_{\text{G}}(\Theta; \mu, \Sigma)\delta(\eta - \eta(\Theta)), \quad (12)$$

with the random vector

$$\Theta = (x_0, y_0, w_1, w_2, \varphi), \quad (13)$$

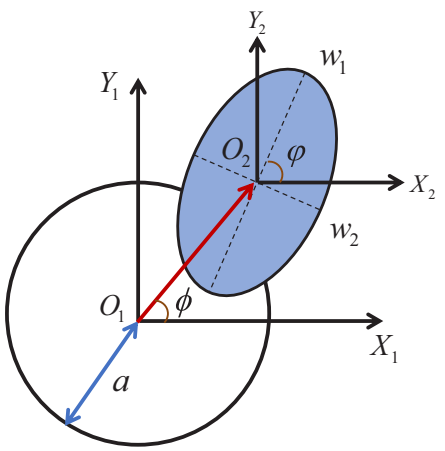

FIG. 2. The elliptic-beam model on the receiving aperture with radius a. w_1 and w_2 denote the semiaxes of arriving elliptic beams. Here w_1 rotates on the angle φ related to the x axis.

where (x_0, y_0) denotes the beam-centroid coordinates at the telescope plane, w_1 and w_2 are the semiaxes of arriving elliptic beams, φ is the orientation angle between the semiaxis w_1 and the x axis, $\eta(\Theta)$ define the relationship between η and v, and $\rho_G(\Theta; \mu, \Sigma)$ is a Gaussian probability density of Θ with the mean value μ and the covariance matrix Σ. However, the model in [49] is based on a horizontal link, where the index of the refraction structure parameter C_n^2 is regarded as a constant. In the satellite-based scenario, C_n^2 is a variable in terms of the altitude of location, so one should update the original model for legitimate use. The update of the elliptic-beam model in satellite-mediated links (both downlink and uplink) is shown in our previous work [50]. The implementation of the updated model for deriving the downlink $\mathcal{P}(\eta)$ is shown in Appendix A.

Note that the simulation parameters shown in Table I are the same as in our previous work, so for the numerical simulation readers can refer to [50]. Since the continuous satellite-mediated link is equivalent to a segmented linear link for less complexity, the parameters C_n^2 and n_0 are constants and denote the equivalent atmosphere parameters for the first 20-km atmospheric thickness above the sea-level site (this thickness includes 95% of total atmospheric effects [16]). In engineering, one can raise the altitude of a ground station for less absorption, scattering, and effects of turbulence. Moreover, the influence of turbulence can be further reduced with various methods, such as AO [51], the receiver diversity [52], and so on [53]. In addition, we use an apparatus-induced boresight error $\alpha = 0.4$ μrad for fine pointing in the downlink approach [47]. This error arises from stress, noise, structure fabrication, and so on in the electronic or mechanical telescope apparatus [21]. Therefore, one can improve the quality of the apparatus for a smaller pointing error. Note that the error caused by turbulence hardly occurs in the downlink approach [54].

B. Excess noise

Next, we discuss the excess noise in the downlink scenario. We mainly consider the noise from background light, which was discussed in our previous work [46]. We present the model of background noise in Appendix B and use the result 5.9622×10^{-6} and 0.6062 shot-noise units for nighttime and daytime scenarios, respectively. Note that we consider the worst-case scenarios with maximal background noise; therefore, the field of view Ω_{fov} of the receiver telescope is set to π. In practice, a smaller telescope introduces less background noise at the receiver but reduces the transmittance of quantum light at the same time [55]. Moreover, one can reduce background noise by AO acting as a spatial filter, while the spectral filtering of the optical signal from the orbiting satellite is useless due to the Doppler effect [56].

In addition, the CVQT protocol requires a LO for homodyne detection [57]. A copropagating LO, suffering from turbulence, shows time-of-arrival fluctuation and leads to a mismatch between the signal and LO [21]. This problem introduces an additional noise even if we consider ideal homodyne detection for the Bell measurement. Fortunately, such noise can be avoided by using a LO, where one can enable reliable coherent detection using a LO generated on the receiver side with an individual laser [58]. Therefore, the noise caused by a copropagating LO is ignored in the following. Note that the LO scheme has a trade-off because part of the signal would be split off for the lock phase; however, such an analysis is beyond the scope of this work.

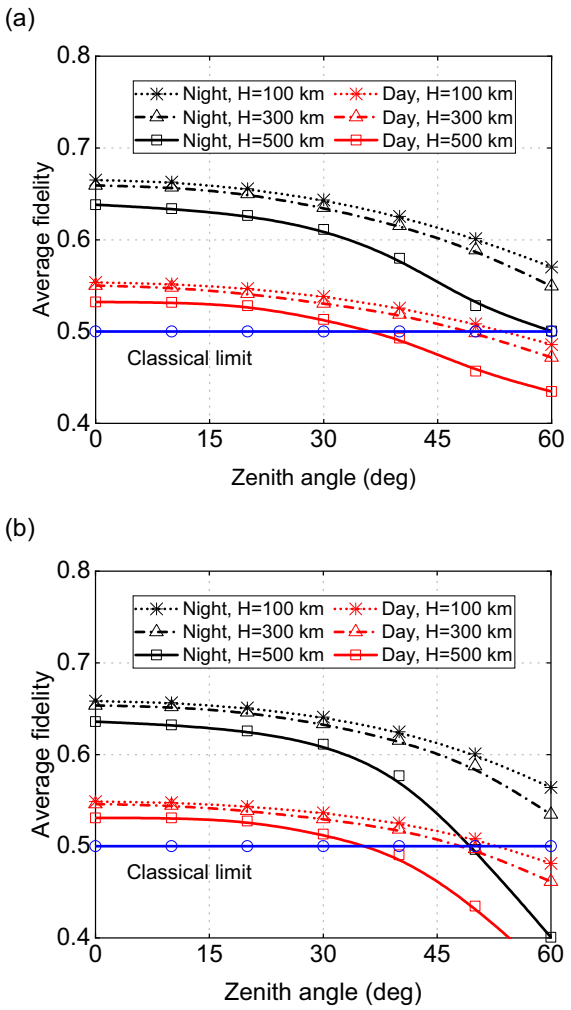

FIG. 3. The average fidelity varying with zenith angle (a) with squeezing optimization and (b) without squeezing optimization. In (a) and (b), the classical limit of teleportation is $\mathcal{F}_{\text{limit}} = 0.5$.

C. Fidelity

To evaluate the effectiveness of the protocol, numerical simulations of average fidelity during both nighttime and daytime are demonstrated. Note that we can achieve fidelity of 0.5 for teleporting coherent states with local operations and classical communication without entanglement [59]. Therefore, quantum teleportation is effective only when the fidelity is larger than the classical limit $\mathcal{F}_{\text{limit}} = 0.5$. Furthermore, an EPR state with too strong squeezing might disentangle faster in uncorrelated loss channels [60]. Figure 1 is a natural example of uncorrelated loss channels, where Bob keeps the mode b location without losses and a remote receiver of mode a, connected via downlink. Hence, we consider the optimization of the squeezing parameter in the following.

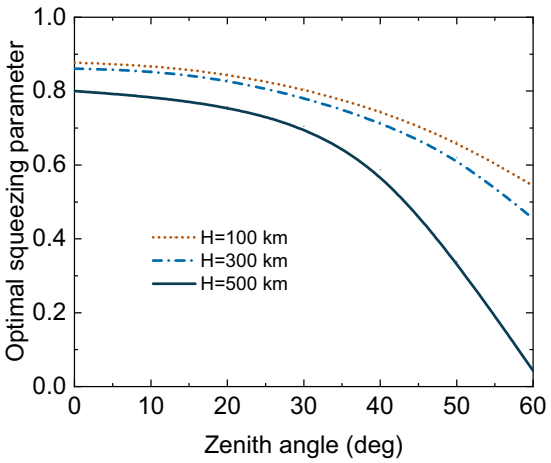

FIG. 4. Optimal squeezing parameter versus zenith angle at different satellite altitudes during nighttime.

The average fidelity $\mathcal{F}_{\text{ave}}$ as a function of zenith angle ζ for different satellite altitudes is shown in Fig. 3(a). Here the squeezing parameter is optimal for each zenith angle. We find that the nighttime average fidelity for all satellite altitudes is above the classical limit, which manifests the effectiveness of our protocol. For the daytime situation, the effectiveness appears when the zenith angle is less than 53°, 49°, and 35° under a 100-, 300-, and 500-km satellite altitude, respectively. Note that a large effective zenith angle means stronger resistance to environmental effects and longer operation time during a single communication cycle. In addition, it is hard for the DV protocol to realize daytime operation without enhancement [29]; therefore, the results show the central role of the proposed protocol for building global-scale quantum networks without both the uplink limit and background-radiation constraints. Figure 3(b) shows the simulations without squeezing optimization, and the squeezing parameter r is set to 0.7. Results show that squeezing optimization improves average fidelity, especially when the satellite altitude rises to 500 km.

Figure 4 reveals the relationship between the optimal squeezing parameter r_{opt} and zenith angle ζ for different satellite altitudes. Here we present the results for the nighttime scenario as an example. A negative correlation is found between the optimal squeezing parameter and the zenith angle at all altitudes. For a fixed zenith angle, the optimal squeezing parameter falls as the satellite altitude rises. Note that both larger zenith angle and higher satellite altitude suggest more serious turbulence effects. Therefore, the optimal squeezing parameter tends to be a small value when the turbulence effects go up.

IV. ENHANCED STRATEGIES

In this section, we propose enhanced strategies to improve the average fidelity of satellite-mediated teleportation. The main resource of teleportation is Gaussian entanglement [2]; therefore, the fidelity can be enhanced by the following strategies. Note that other methods which can preserve Gaussian entanglement also have the potential to enhance the proposed protocol.

A. Active attenuation

As is known, increasing the correlation of two modes in a two-mode Gaussian state is beneficial to the preservation of entanglement [60]. Therefore, we propose an enhanced strategy by increasing the correlation between the downlink and the channel of mode b. The proposed strategy, called the active-attenuation scheme, is shown in Figs. 1(b) and 1(c). A channel monitor is located at the ground station to measure the real-time transmittance of the downlink, and then the side information is broadcasted to Bob via a classical channel. On Bob's side, a variable optical attenuator (VOA) adds adaptive attenuation in terms of real-time transmittance so that the channel of mode b has the same transmittance with the downlink. Hence, the uncorrelated channels turn out to be fully correlated channels and so, as a consequence, preserve entanglement.

Next, we derive the fidelity of the active-attenuation scheme. Mathematically, the added attenuation will affect the blocks of mode b in Eq. (5) and the correlation between two modes. Therefore, the covariance matrix $\mathcal{U}_1$ turns out to be a new covariance matrix given by

$$\mathcal{U}_2=\begin{bmatrix}\tilde{A}\mathbf{I} & \tilde{C}\mathbf{R}\\ \tilde{C}\mathbf{R} & \tilde{B}\mathbf{I}\end{bmatrix}, \tag{14}$$

where $\tilde{A}=A$, $\tilde{B}=\eta\cosh(2r)+1-\eta$, and $\tilde{C}=\eta\sinh(2r)$. Here we assume the VOA only reduces the transmittance without introducing additional excess noise. Then, the fidelity with added attenuation under deterministic losses is given by

$$\mathcal{F}=\frac{1}{2+\eta\cosh(2r)-\eta-\eta\sinh(2r)}. \tag{15}$$

Similarly, the average fidelity under fluctuating losses can be derived in terms of Eq. (11).

Figure 5 shows the average fidelity $\mathcal{F}_{\text{ave}}$ of the active-attenuation scheme as a function of zenith angle ζ considering the effect of the squeezing parameter. The results show that the influence of squeezing parameters on the active-attenuation scheme cannot be neglected. The active-attenuation scheme manifests superior performance under higher losses ($H=500$ km, $\zeta>42°$) only when the squeezing parameter is set to 0.7. If a higher squeezing parameter is used ($r=1.5$), the average fidelity of the active-attenuation scheme never falls below the classical limit, which is not preserved for the no-attenuation scheme. This is because higher squeezing (higher mean photon number in two modes) renders the quantum state more sensitive to losses, so as a consequence, the asymmetry of the state is more pronounced. However, symmetry shows benefits for teleportation [61]. Therefore, the active-attenuation scheme leads to a more pronounced improvement under a higher squeezing parameter.

B. Quantum catalysis

In addition, our previous works [62–64] showed that the quantum catalysis (QC) operation can improve the entanglement property of the EPR state, providing a promising solution to enhance teleportation. Figure 1(d) illustrates the schematic of the QC-based scheme. Here we analyze the case of zero-photon catalysis (ZPC). Accurately, mode a is sent

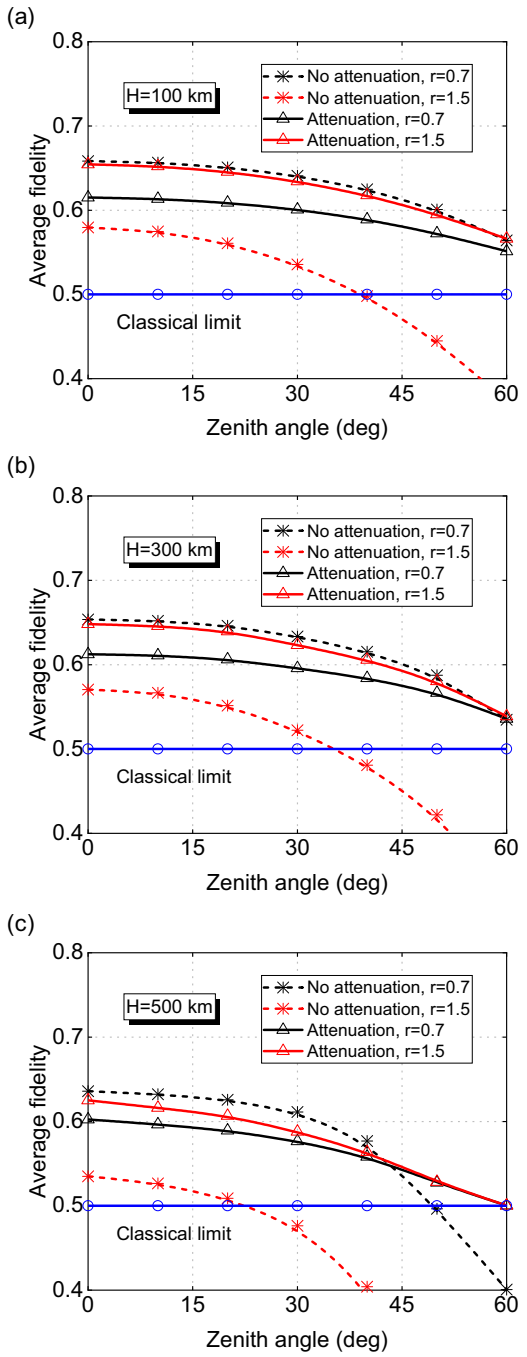

FIG. 5. The average fidelity of the active-attenuation scheme vs zenith angle for different satellite altitudes and squeezing parameters. From top to bottom, the satellite altitude H is equal to 100, 300, and 500 km. Dashed lines represent the case without attenuation.

to one of the input ports of the asymmetrical beam splitter (ABS) before transmission and is modified by an auxiliary zero-photon state. Then, the ZPC operation postselects the ABS output by conditional detection of the zero photon. In an ideal case, the auxiliary zero-photon state will not be destroyed at all, and the photon-number-resolving detector at the corresponding output ports can register zero photons. Hence, the ZPC operation happens to be a zero-energy-input

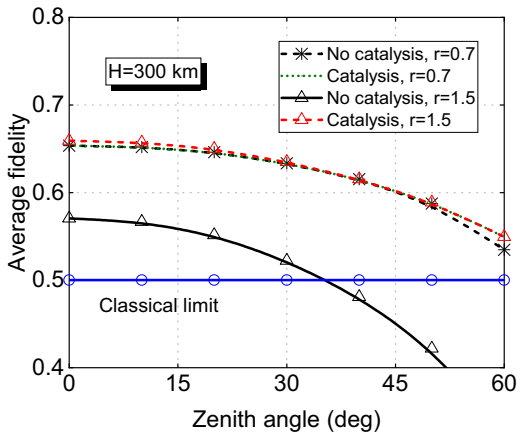

FIG. 6. The average fidelity of the ZPC scheme vs zenith angle for different squeezing parameters. The transmittance of the ABS has been optimized.

operation that does not engender the consumption of external energy.

Next, we derive the fidelity of the ZPC-based scheme. The CF of the EPR state after the ZPC operation becomes (see Appendix C for details)

$$\Phi(\xi_a,\xi_b)=\frac{Z(\xi_a,\xi_b)}{Z(0,0)}\Phi_{\mathrm{EPR},\bar{r}}(\xi_a,\xi_b), \tag{16}$$

where $\Phi_{\mathrm{EPR},\bar{r}}(\xi_a,\xi_b)$ is the CF of the EPR state with a modified squeezing parameter satisfying $\tanh(\bar{r})=\tanh(r)\sqrt{\eta_0}$ and $Z(\xi_a,\xi_b)$ is the term resulting from the ZPC operation given by

$$Z(\xi_a,\xi_b)=\frac{1-\tanh^2(r)}{1-\tanh^2(\bar{r})}. \tag{17}$$

$Z(0,0)$ denotes the success probability of the ZPC operation, which can be expressed as

$$Z(0,0)=\frac{2}{E}, \tag{18}$$

where $E=1+\eta_0+\gamma\cosh(2r)$. Then, the fidelity of the ZPC-based scheme under deterministic losses is derived from Eq. (7), which can be expressed as

$$\mathcal{F}=\frac{E}{2E+\eta_0(\eta+1)[\cosh(2r)-1]-2\sqrt{\eta\eta_0}\sinh(2r)}. \tag{19}$$

Finally, the average fidelity with fluctuating losses can be derived in terms of Eq. (11).

Figure 6 shows the average fidelity $\mathcal{F}_{\mathrm{ave}}$ of the ZPC-based scheme as a function of zenith angle ζ considering the effect of the squeezing parameter. Here we present the results of the nighttime situation with $H=300$ km. The ABS transmittance is optimal for each zenith angle. Results show that the influence of the squeezing parameter cannot be neglected. The larger the squeezing parameter is, the more pronounced the ZPC-induced improvement is. When the squeezing parameter equals 0.7, the ZPC-based scheme shows enhancement only if the zenith angle is more than 45°. Moreover, the maximal fidelity enhancement was achieved at $\zeta=60°$ with an

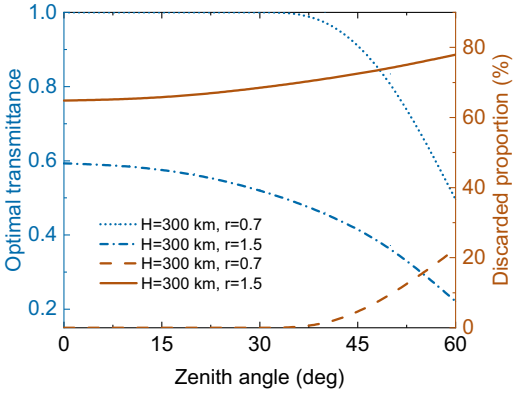

FIG. 7. Optimal transmittance of the ABS vs zenith angle and the corresponding discarded proportion.

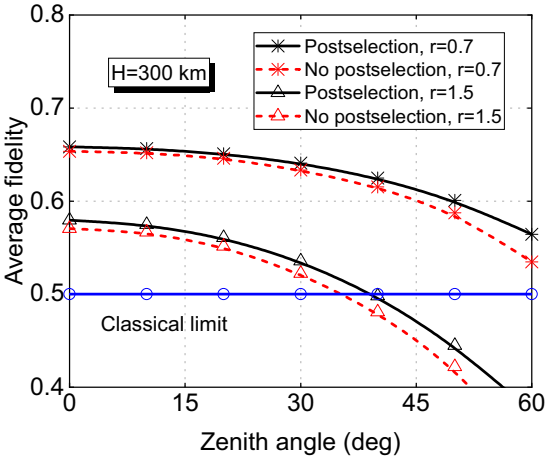

FIG. 8. The average fidelity of the postselection scheme vs zenith angle for different squeezing parameters.

improvement of 0.15. If a squeezing parameter of 1.5 is used, the enhancement can be improved. In this case, the average fidelity never drops below the classical limit with the help of ZPC operation, while it drops to the classical limit at 35° with no catalysis scheme.

Figure 7 shows the optimal ABS transmittance, along with the corresponding discard proportion, as a function of the zenith angle ζ. Note that the discard proportion is related to the success probability of the ZPC operation as shown in Eq. (18) and is independent of the atmosphere transmittance. The optimal ABS transmittance equals 1 in the case of $\zeta \leqslant 35^\circ$ when the squeezing parameter is set to 0.7. In other words, the protocol without the ZPC operation performs better than a ZPC-based one in this case. For a squeezing parameter of 1.5, the ZPC-based scheme shows excellent performance, and a case with a larger zenith angle needs a smaller optimal ABS transmittance.

C. Postselection

The postselection scheme has been shown to improve the performance of free-space continuous-variable QKD in both the asymptotic regime [65] and composable regime [66]. In these references, the system improves the secret key rate by postselecting the events with high transmittance and discards the events under the preset threshold. Then, the preserved events for further tasks have a higher quality of entanglement.

We therefore consider the technique of postselection for teleportation enhancement. We set a transmittance threshold $\eta_{\min}$ before teleportation and monitor the downlink transmittance the same as in the active-attenuation scheme [see Figs. 1(b) and 1(c)]. The ground station discards quantum states with low transmittance ($\eta < \eta_{\min}$) and holds one with higher transmittance for teleportation. From the engineering point of view, postselection is the easiest to implement among the three methods of our work since it off-loads additional processing to the ground station, so it has fewer modifications and less data processing on the satellite side. In engineering, space, power consumption, and computational power or memory are often constrained on a satellite [53]. However, the increase in fidelity from postselection rests on discarding part of the quantum state. Hence, this scheme should strike a trade-off between average fidelity and the discard proportion in practice.

Figure 8 shows the average fidelity $\mathcal{F}_{\text{ave}}$ of the postselection scheme as a function of zenith angle ζ considering the effect of the squeezing parameter. Here we present the results for the nighttime scenario with $H = 300$ km. For a simple and convenient discussion, we ignore the trade-off between average fidelity and discarding quantum states. Hence, the transmittance threshold is optimal for each zenith angle to maximize the average fidelity. We find that the protocol with postselection improves average fidelity under all conditions. This is not only because of the improved average transmittance of preserved quantum states but also because of the reduced transmittance fluctuation. A more intuitive way to understand this effect from channel fluctuation can be given by considering the Simon entanglement criterion [67] in which any two-mode Gaussian state is entangled only if the entanglement-criterion equation is negative. The reduced fluctuation reduces the positive element of the entanglement-criterion equation, preserving its negative value.

Figure 9 shows the optimal threshold η_{opt}, along with the corresponding discard proportion, vs zenith angle ζ. A negative correlation is found between the optimal threshold

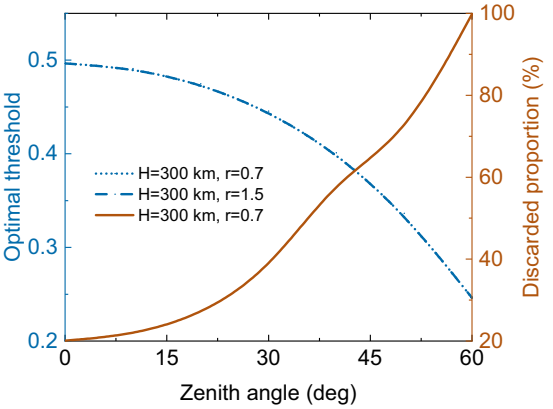

FIG. 9. Optimal threshold vs zenith angle and the corresponding discarded proportion.

and zenith angle. As the zenith angle increases, the discard proportion rises and reaches up to 100% when the zenith angle is 60° (here $\eta_{\text{opt}} = 0.2461$). In addition, no significant correlation is found between the optimal threshold and the squeezing parameter.

V. CONCLUSION

We have suggested the BK-based CVQT protocol to overcome both the uplink limit and background-radiation constraints of satellite-based quantum communication through an unconditional and deterministic transfer. In this protocol, the CV entanglement source is deployed to the quantum satellite; therefore, the teleported quantum state finishes the transmission from the ground to satellite via a favorable downlink. We presented the setup of the protocol and then established the downlink model focusing on atmosphere transmittance and the excess noise from the background light. Accounting for these models, we derived the average fidelity of the protocol for satellites with different altitudes and zenith angles under both nighttime and daytime operation. The results illustrate that the proposed protocol can overcome the uplink limit and achieve effective teleportation even for a satellite at 500-km orbit. Benefiting from coherent detection, the protocol offers effective resistance against background noise, thereby realizing all-day operation. We also investigated that the optimal squeezing parameter of the EPR state tends to a smaller value under stronger turbulence. Furthermore, by preserving Gaussian entanglement in terms of the characteristics of the free-space link, we further improved the average fidelity of the protocol with several strategies, i.e., active attenuation, quantum catalysis, and postselection.

ACKNOWLEDGMENTS

We would like to thank Dr. D. Vasylyev, Dr. M. Bohmann, Q. Peng, and K. Hofmann for helpful discussions. This work is supported by the National Natural Science Foundation of China (Grants No. 61871407 and No. 62101180), the Hunan Provincial Natural Science Foundation of China (Grant No. 2020JJ5088), and the Fundamental Research Funds for the Central Universities (Grant No. 531118010371).

APPENDIX A: THE IMPLEMENTATION OF THE ELLIPTIC-BEAM MODEL

The vector μ of Eq. (13) can be expressed as

$$\mu = \left(\langle x_0\rangle, \langle y_0\rangle, \langle w_1^2\rangle, \langle w_2^2\rangle\right), \tag{A1}$$

where the elements $\langle x_0\rangle = \langle y_0\rangle = 0$. The covariance matrix Σ is given by

$$\Sigma = \begin{bmatrix} \langle x_0^2\rangle & 0 & 0 & 0 \\ 0 & \langle y_0^2\rangle & 0 & 0 \\ 0 & 0 & \langle \Delta w_1^2\rangle & \langle \Delta w_1 \Delta w_2\rangle \\ 0 & 0 & \langle \Delta w_1 \Delta w_2\rangle & \langle \Delta w_2^2\rangle \end{bmatrix}. \tag{A2}$$

The derivation of μ and Σ refer to the Supplemental Material of [49]. In this work, we derive μ and Σ of the downlink scenario with the equivalent atmospheric parameters together with the permittivity fluctuation spectrum [68]

$$\Lambda(\tau) = 0.132 C_n^2 |\tau|^{-\frac{11}{3}} + \frac{2n_0}{\pi k^4} |f_0(\tau; d_{\text{scat}})|^2, \tag{A3}$$

where $k = 2\pi/\lambda$ indicates the wave number, $|\tau| \in [\tau_0, \tau_m]$, with $\tau_0 \in 1/L_0$, and $\tau_m \in 1/l_0$ (l_0 is the inner scale of the turbulence). $f_0(\tau; d_{\text{scat}})$ indicates the amplitude of the wave scattered from a separate particle, whose calculation method can be found in [69]. The last two parameters of μ in the updated model can be calculated as

$$\langle w_i^2\rangle = \frac{4\mathrm{H}^2 \sec^2(\zeta)}{k^2 W_0^2}\left[\frac{\pi}{24} n_0 W_0^2 \sec(\zeta) \frac{\bar{h}^3}{\mathrm{H}^2} + 1.1 C_n^2 k^2 W_0^{\frac{5}{3}} \sec(\zeta) \frac{\bar{h}^{\frac{8}{3}}}{\mathrm{H}^{\frac{5}{3}}} + 1\right], \tag{A4}$$

where $\bar{h} = 20$ km represents the altitude of the layer with main atmosphere effects. For Σ, the factors become

$$\langle x_0^2\rangle = \langle y_0^2\rangle = \alpha H \sec(\zeta), \tag{A5}$$

$$\langle w_i^2\rangle = \frac{4H^2 \sec^2(\zeta)}{k^2 w_0^2}\left[\frac{\pi}{24} n_0 w_0^2 \sec(\zeta) \frac{\bar{h}^3}{H^2} + 1.1 C_n^2 k^2 W_0^{\frac{5}{3}} \sec(\zeta) \frac{\bar{h}^{\frac{8}{3}}}{H^{\frac{5}{3}}} + 1\right]. \tag{A6}$$

Based on the elements above, we can estimate $\mathcal{P}(\eta)$ via the Monte Carlo method. In general, the transmittance η can be estimated by

$$\eta = \vartheta(\zeta)\tilde{\eta} \exp\left\{-\left[\frac{\Xi/a}{\mathbb{A}\left(\frac{2}{W_{\text{eff}}(\varphi-\phi)}\right)}\right]^{\mathbb{B}\left(\frac{2}{W_{\text{eff}}(\varphi-\phi)}\right)}\right\}, \tag{A7}$$

with

$$\vartheta(\zeta) = \exp[-\beta \sec(\zeta)], \tag{A8}$$

where β is the extinction coefficient, $\Xi = (x_0, y_0)$ with the corresponding polar coordinates (Ξ, ϕ), $W_{\text{eff}}(\cdot)$ is the effective spot radius with the deformation effect, and $\tilde{\eta}$ is the transmittance for the centered beam, which can be calculated by

$$\tilde{\eta} = 1 - I_0\left(a^2\left[\frac{w_2^2 - w_1^2}{w_1^2 w_2^2}\right]\right) e^{-a^2 \frac{w_2^2 + w_1^2}{w_1^2 w_2^2}} - 2\left\{1 - e^{-\frac{a^2}{2}\left(\frac{1}{w_1} - \frac{1}{w_2}\right)}\right\} \exp\left\{-\left[\frac{\frac{(w_1+w_2)^2}{|w_1^2 - w_2^2|}}{\mathbb{A}\left(\frac{1}{w_1} - \frac{1}{w_2}\right)}\right]^{\lambda\left(\frac{1}{w_1} - \frac{1}{w_2}\right)}\right\}, \tag{A9}$$

where $\mathbb{A}(\cdot)$ is the scale function and $\mathbb{B}(\cdot)$ is the shape function. The two functions can be expressed as

$$\mathbb{A}(\varsigma) = \left[\ln\left(2\frac{1-\exp\left[-\frac{1}{2}a^2\varsigma^2\right]}{1-\exp[-a^2\varsigma^2]I_0(a^2\varsigma^2)}\right)\right]^{-\frac{1}{\mathbb{B}(\varsigma)}}, \quad \text{(A10)}$$

$$\mathbb{B}(\varsigma) = 2a^2\varsigma^2\frac{\exp(-a^2\varsigma^2)I_1(a^2\xi^2)}{1-\exp(-a^2\varsigma^2)I_0(a^2\varsigma^2)} \times\left[\ln\left(2\frac{1-\exp\left[-\frac{1}{2}a^2\varsigma^2\right]}{1-\exp[-a^2\varsigma^2]I_0(a^2\varsigma^2)}\right)\right]^{-1}, \quad \text{(A11)}$$

where $I_i(\cdot)$ indicates the modified Bessel function of the ith order.

APPENDIX B: BACKGROUND NOISE

In the daytime (nighttime) situation, the main cause of background noise is the sunlight (moonlight) collected by the receiver based on the station on Earth. As the telescope comes close to the surface of Earth, the noise power P received by the telescope can be expressed as [46]

$$P = \Omega_{\text{fov}}A_{\text{rec}}H_bB_{\text{filter}}, \quad \text{(B1)}$$

where the parameters from left to right are field of view, aperture area, the brightness of the sky ground, and filter bandwidth, respectively. The parameter H_b changes with weather conditions, as listed in [48]. Here we use $H_b = 1.5\times10^{-5}$ W m^{-2} Sr μm and $H_b = 1.5$ W m^{-2} Sr μm for nighttime and daytime situations, respectively. Finally, the excess noise is given by

$$\epsilon = \frac{\beta_{\text{eff}}P}{h\upsilon_c}, \quad \text{(B2)}$$

where h denotes Planck's constant, υ_c is the frequency of light, and β_{eff} is the effective sampling period of the homodyne detector, which is set to 1 ns [46].

APPENDIX C: THE CF OF THE EPR STATE AFTER ZPC OPERATION

Here we derive the CF of the EPR state after ZPC operation. Theoretically, the input-output relation of the ZPC operation under density-operator representation can be expressed as

$$\rho_{\text{out},b} = \text{Tr}_{b'}[B\rho_{\text{in},b}|0\rangle_{b'b'}\langle 0|S^\dagger|0\rangle_{b'b'}\langle 0|], \quad \text{(C1)}$$

where S denotes the beam-splitter operator related to the ABS transmittance η_0. In terms of the Weyl expansion of the density operator [70], the CF corresponding to $\rho_{\text{out},b}$ is given by

$$\Phi_{\text{out}}(\xi) = \int\frac{d^2\kappa}{\pi\gamma}\Phi_{\text{in}}(\kappa)\Phi_0(\kappa_1)\Phi_0(\kappa_2), \quad \text{(C2)}$$

where $\kappa_1 = \xi/\sqrt{\gamma} - \kappa\sqrt{\eta_0/\gamma}$, $\kappa_2 = \kappa/\sqrt{\gamma} - \xi\sqrt{\eta_0/\gamma}$, $\gamma = 1-\eta_0$, Φ_{in} is the CF of the input mode, and Φ_0 is the CF of the zero-photon Fock state, which has the form

$$\Phi_0(\kappa_{1,2}) = e^{-\frac{1}{2}|\kappa_{1,2}|^2}L_0(|\kappa_{1,2}|^2), \quad \text{(C3)}$$

where $L_0(\cdot)$ are the Laguerre polynomials. Note that we have used the following integration formula:

$$\int\frac{d^2\gamma}{\pi}e^{-x|\gamma|+y\gamma+z\gamma^*} = \frac{1}{x}e^{\frac{yz}{x}}. \quad \text{(C4)}$$

[1] N. Gisin and R. Thew, Quantum communication, Nat. Photon. **1**, 165 (2007).

[2] S. Pirandola, J. Eisert, C. Weedbrook, A. Furusawa, and S. L. Braunstein, Advances in quantum teleportation, Nat. Photon. **9**, 641 (2015).

[3] F. Xu, X. Ma, Q. Zhang, H.-K. Lo, and J.-W. Pan, Secure quantum key distribution with realistic devices, Rev. Mod. Phys. **92**, 025002 (2020).

[4] Q. Liao, G. Xiao, C.-G. Xu, Y. Xu, and Y. Guo, Discretely modulated continuous-variable quantum key distribution with an untrusted entanglement source, Phys. Rev. A **102**, 032604 (2020).

[5] Q. Liao, G. Xiao, H. Zhong, and Y. Guo, Multi-label learning for improving discretely-modulated continuous-variable quantum key distribution, New J. Phys. **22**, 083086 (2020).

[6] Q. Liao, H. Liu, L. Zhu, and Y. Guo, Quantum secret sharing using discretely modulated coherent states, Phys. Rev. A **103**, 032410 (2021).

[7] R. Jozsa, D. S. Abrams, J. P. Dowling, and C. P. Williams, Quantum Clock Synchronization Based on Shared Prior Entanglement, Phys. Rev. Lett. **85**, 2010 (2000).

[8] C. L. Degen, F. Reinhard, and P. Cappellaro, Quantum sensing, Rev. Mod. Phys. **89**, 035002 (2017).

[9] W. K. Wootters and W. H. Zurek, A single quantum cannot be cloned, Nature (London) **299**, 802 (1982).

[10] H.-J. Briegel, W. Dür, J. I. Cirac, and P. Zoller, Quantum Repeaters: The Role of Imperfect Local Operations in Quantum Communication, Phys. Rev. Lett. **81**, 5932 (1998).

[11] M. Zukowski, A. Zeilinger, M. A. Horne, and A. K. Ekert, "Event-Ready-Detectors" Bell Experiment via Entanglement Swapping, Phys. Rev. Lett. **71**, 4287 (1993).

[12] C. H. Bennett, G. Brassard, S. Popescu, B. Schumacher, J. A. Smolin, and W. K. Wootters, Purification of Noisy Entanglement and Faithful Teleportation via Noisy Channels, Phys. Rev. Lett. **76**, 722 (1996).

[13] S.-J. Yang, X.-J. Wang, X.-H. Bao, and J.-W. Pan, An efficient quantum light–matter interface with sub-second lifetime, Nat. Photon. **10**, 381 (2016).

[14] M. Lucamarini, Z. L. Yuan, J. F. Dynes, and A. J. Shields, Overcoming the rate–distance limit of quantum key distribution without quantum repeaters, Nature (London) **557**, 400 (2018).

[15] S. Pirandola, Satellite quantum communications: Fundamental bounds and practical security, Phys. Rev. Research **3**, 023130 (2021).

[16] C. Liorni, H. Kampermann, and D. Bruß, Satellite-based links for quantum key distribution: Beam effects and weather dependence, New J. Phys. **21**, 093055 (2019).

[17] S.-K. Liao *et al.*, Satellite-to-ground quantum key distribution, Nature (London) **549**, 43 (2017).

[18] J. Yin *et al.*, Satellite-based entanglement distribution over 1200 kilometers, Science **356**, 1140 (2017).

[19] J.-G. Ren *et al.*, Ground-to-satellite quantum teleportation, Nature (London) **549**, 70 (2017).

[20] H. Takenaka, A. Carrasco-Casado, M. Fujiwara, M. Kitamura, M. Sasaki, and M. Toyoshima, Satellite-to-ground quantum-limited communication using a 50-kg-class microsatellite, Nat. Photon. **11**, 502 (2017).

[21] L. C. Andrews and R. L. Phillips, *Laser Beam Propagation through Random Media*, 2nd ed. (SPIE, Bellinghan, 2005).

[22] J. P. Bourgoin, E. Meyer-Scott, B. L. Higgins, B. Helou, C. Erven, H. Huebel, B. Kumar, D. Hudson, I. D'Souza, R. Girard *et al.*, A comprehensive design and performance analysis of low earth orbit satellite quantum communication, New J. Phys **15**, 023006 (2013).

[23] C. J. Pugh, J.-F. Lavigne, J.-P. Bourgoin, B. L. Higgins, and T. Jennewein, Adaptive optics benefit for quantum key distribution uplink from ground to a satellite, Adv. Opt. Technol. **9**, 263 (2020).

[24] D. Vasylyev, W. Vogel, and F. Moll, Satellite-mediated quantum atmospheric links, Phys. Rev. A **99**, 053830 (2019).

[25] M. D. Oliker and M. T. Gruneisen, How much value does adaptive optics add to a satellite QKD uplink? Proc. SPIE **11167**, 1116706 (2019).

[26] T. Jennewein, J. P. Bourgoin, B. Higgins, C. Holloway, E. Meyer-Scott, C. Erven, B. Heim, Z. Yan, H. Hübel, G. Weihs, E. Choi, I. d'Souza, D. Hudson, and R. Laflamme, QEYSSAT: A mission proposal for a quantum receiver in space, Proc. SPIE **8997**, 89970A (2014).

[27] M. Huo, J. Qin, J. Cheng, Z. Yan, Z. Qin, X. Su, X. Jia, C. Xie, and K. Peng, Deterministic quantum teleportation through fiber channels, Sci. Adv. **4**, eaas9401 (2018).

[28] D. E. Bruschi, T. C. Ralph, I. Fuentes, T. Jennewein, and M. Razavi, Spacetime effects on satellite-based quantum communications, Phys. Rev. D **90**, 045041 (2014).

[29] S.-K. Liao *et al.*, Long-distance free-space quantum key distribution in daylight towards intersatellite communication, Nat. Photon. **11**, 509 (2017).

[30] A. Furusawa, J. L. Sorensen, S. L. Braunstein, C. A. Fuchs, H. J. Kimble, and E. S. Polzik, Unconditional quantum teleportation, Science **282**, 706 (1998).

[31] N. Hosseinidehaj, Z. Babar, R. Malaney, S. X. Ng, and L. Hanzo, Satellite-based continuous-variable quantum communications: State-of-the-art and a predictive outlook, Commun. Surv. Tutorials **21**, 881 (2019).

[32] Z. Yan, J.-L. Qin, Z.-Z. Qin, X.-L. Su, X.-J. Jia, C.-D. Xie, and K.-C. Peng, Generation of non-classical states of light and their application in deterministic quantum teleportation, Fundam. Res. **1**, 43 (2021).

[33] S. Wang, P. Huang, T. Wang, and G. Zeng, Feasibility of All-Day Quantum Communication with Coherent Detection, Phys. Rev. Appl. **12**, 024041 (2019).

[34] S. L. Braunstein and H. J. Kimble, Teleportation of Continuous Quantum Variables, Phys. Rev. Lett. **80**, 869 (1998).

[35] P. Marian and T. A. Marian, Continuous-variable teleportation in the characteristic-function description, Phys. Rev. A **74**, 042306 (2006).

[36] F. Dell'Anno, S. De Siena, and F. Illuminati, Realistic continuous-variable quantum teleportation with non-Gaussian resources, Phys. Rev. A **81**, 012333 (2010).

[37] E. Anisimova, B. L. Higgins, J.-P. Bourgoin, M. Cranmer, E. Choi, D. Hudson, L. P. Piche, A. Scott, V. Makarov, and T. Jennewein, Mitigating radiation damage of single photon detectors for space applications, EPJ Quantum Technol. **4**, 10 (2017).

[38] D. K. L. Oi, A. Ling, J. A. Grieve, T. Jennewein, A. N. Dinkelaker, and M. Krutzik, Nanosatellites for quantum science and technology, Contemp. Phys. **58**, 25 (2017).

[39] R. Jozsa, Fidelity for mixed quantum states, J. Mod. Opt. **41**, 2315 (1994).

[40] A. V. Chizhov, L. Knöll, and D.-G. Welsch, Continuous-variable quantum teleportation through lossy channels, Phys. Rev. A **65**, 022310 (2002).

[41] J. Fiurášek, Improving the fidelity of continuous-variable teleportation via local operations, Phys. Rev. A **66**, 012304 (2002).

[42] D. Yu. Vasylyev, A. A. Semenov, and W. Vogel, Toward Global Quantum Communication: Beam Wandering Preserves Nonclassicality, Phys. Rev. Lett. **108**, 220501 (2012).

[43] V. I. Tatarskii, *The Effects of the Turbulent Atmosphere on Wave Propagation* (Israel Program for Scientific Translations, Jerusalem, 1971).

[44] W. Huang, Y. Mao, C. Xie, and D. Huang, Quantum hacking of free-space continuous-variable quantum key distribution by using a machine-learning technique, Phys. Rev. A **100**, 012316 (2019).

[45] S. Wang, P. Huang, T. Wang, and G. Zeng, Atmospheric effects on continuous-variable quantum key distribution, New J. Phys. **20**, 083037 (2018).

[46] Y. Guo, C. Xie, P. Huang, J. Li, L. Zhang, D. Huang, and G. Zeng, Channel-parameter estimation for satellite-to-submarine continuous-variable quantum key distribution, Phys. Rev. A **97**, 052326 (2018).

[47] T. Jono, Y. Takayama, K. Shiratama, I. Mase, B. Demelenne, Z. Sodnik, A. Bird, M. Toyoshima, H. Kunimori, D. Giggenbach, N. Perlot, M. Knapek, and K. Ara, Overview of the inter-orbit and the orbit-to-ground laser communication demonstration by OICETS, Proc. SPIE **6457**, 645702 (2007).

[48] E. Miao, Z. Han, S. Gong, T. Zhang, D. Diao, and G. Guo, Background noise of satellite-to-ground quantum key distribution, New J. Phys. **7**, 215 (2005).

[49] D. Vasylyev, A. A. Semenov, and W. Vogel, Atmospheric Quantum Channels with Weak and Strong Turbulence, Phys. Rev. Lett. **117**, 090501 (2016).

[50] Z. Zuo, Y. Wang, D. Huang, and Y. Guo, Atmospheric effects on satellite-mediated continuous-variable quantum key distribution, J. Phys. A **53**, 465302 (2020).

[51] G. Chai, Z. Cao, W. Liu, S. Wang, P. Huang, and G. Zeng, Parameter estimation of atmospheric continuous-variable quantum key distribution, Phys. Rev. A **99**, 032326 (2019).

[52] R. Yuan and J. Cheng, Free-space optical quantum communications in turbulent channels with receiver diversity, IEEE Trans. Commun. **68**, 5706 (2020).

[53] J. S. Sidhu, S. K. Joshi, M. Gündoğan, T. Brougham, D. Lowndes, L. Mazzarella, M. Krutzik, S. Mohapatra, D. Dequal, G. Vallone *et al.*, Advances in space quantum communications, IET Quant. Comm. 1 (2021).

[54] D. Dequal, L. T. Vidarte, V. R. Rodriguez, G. Vallone, P. Villoresi, A. Leverrier, and E. Diamanti, Feasibility of satellite-to-ground continuous-variable quantum key distribution, npj Quantum Inf. **7**, 1 (2021).

[55] S. Pirandola, Limits and security of free-space quantum communications, Phys. Rev. Research **3**, 013279 (2021).

[56] M. T. Gruneisen, M. L. Eickhoff, S. C. Newey, K. E. Stoltenberg, J. F. Morris, M. Bareian, M. A. Harris, D. W. Oesch, M. D. Oliker, M. B. Flanagan, B. T. Kay, J. D. Schiller, and R. N. Lanning, Adaptive-Optics-Enabled Quantum Communication: A Technique for Daytime Space-to-Earth Links, Phys. Rev. Appl. **16**, 014067 (2021).

[57] A. A. Semenov, F. Töppel, D. Yu Vasylyev, H. V. Gomonay, and W. Vogel, Homodyne detection for atmosphere channels, Phys. Rev. A **85**, 013826 (2012).

[58] B. Qi, P. Lougovski, R. Pooser, W. Grice, and M. Bobrek, Generating the Local Oscillator "Locally" in Continuous-Variable Quantum Key Distribution Based on Coherent Detection, Phys. Rev. X **5**, 041009 (2015).

[59] S. L. Braunstein, C. A. Fuchs, H. J. Kimble, and P. van Loock, Quantum versus classical domains for teleportation with continuous variables, Phys. Rev. A **64**, 022321 (2001).

[60] M. Bohmann, A. A. Semenov, J. Sperling, and W. Vogel, Gaussian entanglement in the turbulent atmosphere, Phys. Rev. A **94**, 010302(R) (2016).

[61] K. Hofmann, A. A. Semenov, W. Vogel, and M. Bohmann, Quantum teleportation through atmospheric channels, Phys. Scr. **94**, 125104 (2019).

[62] Y. Guo, W. Ye, H. Zhong, and Q. Liao, Continuous-variable quantum key distribution with non-Gaussian quantum catalysis, Phys. Rev. A **99**, 032327 (2019).

[63] W. Ye, H. Zhong, Q. Liao, D. Huang, L. Hu, and Y. Guo, Improvement of self-referenced continuous-variable quantum key distribution with quantum photon catalysis, Opt. Express **27**, 17186 (2019).

[64] Z. Zuo, Y. Wang, Y. Mao, W. Ye, L. Hu, D. Huang, and Y. Guo, Quantum catalysis-assisted attenuation for improving free-space continuous-variable quantum key distribution, J. Phys. B **53**, 185501 (2020).

[65] V. C. Usenko, B. Heim, C. Peuntinger, C. Wittmann, C. Marquardt, G. Leuchs, and R. Filip, Entanglement of Gaussian states and the applicability to quantum key distribution over fading channels, New J. Phys. **14**, 093048 (2012).

[66] N. Hosseinidehaj, N. Walk, and T. C. Ralph, Composable finite-size effects in free-space continuous-variable quantum-key-distribution systems, Phys. Rev. A **103**, 012605 (2021).

[67] R. Simon, Peres-Horodecki Separability Criterion for Continuous Variable Systems, Phys. Rev. Lett. **84**, 2726 (2000).

[68] D. Vasylyev, A. A. Semenov, W. Vogel, K. Günthner, A. Thurn, Ö. Bayraktar, and Ch. Marquardt, Free-space quantum links under diverse weather conditions, Phys. Rev. A **96**, 043856 (2017).

[69] H. van de Hulst, *Light Scattering by Small Particles* (Dover, New York, 2012).

[70] L. Hu, M. Al-amri, Z. Liao, and M. S. Zubairy, Continuous-variable quantum key distribution with non-Gaussian operations, Phys. Rev. A **102**, 012608 (2020).